GEOSAT Follow-On Water Vapor Radiometer: Performance With a Shared Active/Passive Antenna

Christopher S. Ruf, *Fellow, IEEE*, and April M. Warnock

***Abstract*—The GEOSAT Follow-On mission marks the first time that an Earth-orbiting microwave radiometer and radar have shared the same antenna. The antenna design must simultaneously accommodate the radar's high-gain requirement and the high beam efficiency needed by the radiometer. Guaranteeing sufficiently high isolation between the radar transmitter and the radiometer receivers is also a critical part of the antenna design. The radiometer receiver includes a transmitter blanking circuit to further mitigate possible radar interference. Preflight and on-orbit tests of the antenna and radiometer receivers and an evaluation of end-to-end radiometric accuracy are presented. Together, they demonstrate that the shared-antenna approach can be implemented without compromising radiometric performance.**

***Index Terms*—Altimeter, calibration/validation, Geodetic Satellite (GEOSAT), microwave radiometer.**

I. Introduction

THE GEOSAT Follow-On (GFO) mission is intended to continue the oceanographic work begun with the earlier GEOSAT Mission [1], [4] by developing a prototype for an operational ocean topology satellite. GFO was launched on February 10, 1998, from Vandenberg Air Force Base, CA. It is in an orbit similar to that of the original GEOSAT (800-km altitude, 108° inclination, 0.001 eccentricity, 100-min period, and 17-day exact repeat cycle). The satellite carries a radar altimeter, operating at 13.5 GHz, to measure round-trip time of flight and infer sea level and a water vapor radiometer (WVR), operating at 22.2 and 37.0 GHz, to measure integrated water vapor burden in the atmosphere and correct for the reduction in propagation speed of the radar signal due to the humidity (henceforth referred to as *path delay*) [8]. The altimeter was designed and built by E-Systems, ECI Division, St. Petersburg, FL (now Raytheon E-Systems). The radiometer receivers were designed and built by AIL Systems, Inc., Deer Park, NY (now the EDO Electronic Systems Group). The GFO prime contractor and system integrator was Ball Aerospace and Technologies Corporation, Boulder, CO.

A number of other satellite altimeter missions have carried radiometers to similarly provide a path delay correction. These include the Scanning Multichannel Microwave Radiometer on SeaSat and Nimbus 7 [7], [14], the Along-Track Scanning Radiometer/Microwave Radiometer on the European Remote Sensing 1 and 2 satellites (ERS 1/2) [2], [13], the TOPEX Microwave Radiometer (TMR) on the TOPEX/Poseidon satellite [6], [9], [10], and the Jason-1 Microwave Radiometer [3]. In each of these cases, the altimeter and radiometer were independent instruments with their own antenna subsystems. While this provides for a naturally high-level isolation between the high-power transmissions generated by the altimeter and the extremely sensitive receivers in the radiometer, it is at the same time both inconvenient and wasteful. The inconvenience arises from the fact that both sensors' antenna beams need to be coaligned in a nadir-pointing direction. Considerable care must be taken in the mechanical mounting and electrical boresighting of the two antennas to assure this. The waste is simply one of real estate. A single antenna is lighter and cheaper and takes up much less space.

The use of two separate antennas is, in large part, a result of heritage and history considerations. Two different antenna designs were available at the time, which individually provided either the gain needed by the radar or the beam efficiency required of the radiometer. A shared antenna would have required significant new design work. Separate antennas also allowed for the use of heritage radiometer electronics designs. A shared antenna increases the possibility of interference between radar and radiometer. In order to protect against possible levels of interference in excess of the natural noise floor of the radiometer, it is prudent to add a "transmitter blanking" circuit to the integrator stage of the radiometer. Radiometers with such a design had not previously been flown in space. In addition, the GFO WVR has only two frequency channels, at 22.2 and 37.0 GHz, rather than the three frequencies used by most other radiometers for altimetry missions. Three channel systems are used to independently correct path delay estimates for the effects of cloud liquid water and ocean surface wind speed. The GFO retrieval uses its altimeter radar cross-sectional measurements to estimate ocean surface wind speed and thus eliminates the need for a third channel [8]. The retrieval uses the same atmospheric absorption models for water vapor and oxygen, and the same ocean surface emission models as are used by the TOPEX and Jason missions, with appropriate corrections for the frequency differences [5], [15]. Because GFO was a prototype for an operational ocean altimetry platform, significant new design and development was possible to reduce

Manuscript received September 18, 2006; revised November 18, 2006.

The authors are with the Space Physics Research Laboratory, Department of Atmospheric, Oceanic, and Space Sciences, University of Michigan, Ann Arbor, MI 48109-2143 USA (e-mail: cruf@umich.edu).

Color versions of one or more of the figures in this paper are available online at http://ieeexplore.ieee.org.

Digital Object Identifier 10.1109/TGRS.2006.890415

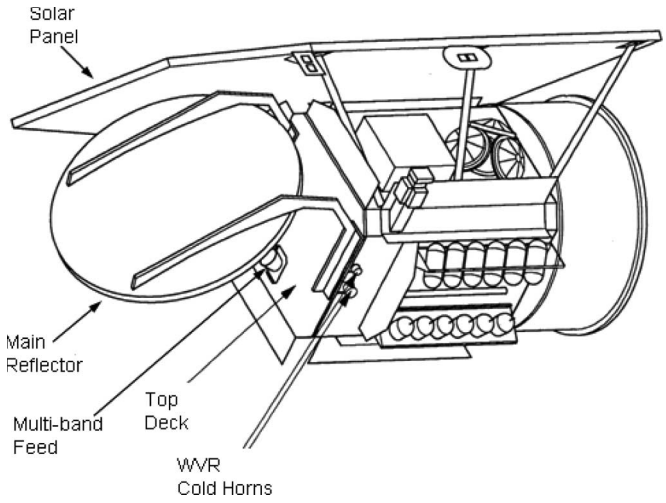

Fig. 1. GFO satellite. The multiband feed and main reflector are shared by the two-channel WVR and the single-channel radar altimeter.

complexity and lower the recurring cost of subsequent units. This drove the decision to use a shared active/passive antenna and to reduce the radiometer channel count from three to two frequencies. The result was a smaller, lighter, and cheaper combined altimeter/radiometer.

Details of the instrument design are presented in Section II, with emphasis on the shared antenna. Following that are details concerning on-orbit performance assessments made during the early commissioning phase of the mission and made over the entire mission lifetime to date. Evaluations of on-orbit performance are presented, which confirm that radiometric accuracy is largely unaffected by the sharing of the antenna with the radar altimeter.

II. Radiometer Design and Prelaunch Test Results

A drawing of the GFO spacecraft is shown in Fig. 1, with relevant features of the WVR noted—in particular, the shared radar/radiometer antenna and feed horn. Also noted is the location of the cold horns that view space and provide the radiometer a cold calibration reference brightness temperature.

A. Radar/Radiometer Antenna

The GFO altimeter/radiometer antenna is designed to simultaneously meet both the altimeter gain and radiometer beam efficiency requirements. The offset parabolic reflector has a 105-cm diameter. The reflector is fed by a trifrequency machined aluminum horn operating at 13.5, 22.2, and 37 GHz with linear polarization. Both the main reflector and feed were designed and built by Ball Aerospace and Technologies Corporation, Broomfield, CO. The peak gain of the 13.5-GHz altimeter channel is 40.25 dBi. The half-power beamwidths of the two radiometer channels are 1.01° and 0.63° at 22.2 and 37 GHz, respectively. The antenna beam fractions of the two radiometer channels, which are integrated over all azimuthal angles at specific ranges of off-boresight angles, are critical specifications that influence the calibration accuracy of the derived radiometer brightness temperatures. The beam fractions at 22.2 and 37 GHz in the main beam and near sidelobes—from boresight to 10° off boresight—are 98.72% and 99.38%, respectively. The beam fractions of the on-Earth far sidelobes—from 10° off boresight to the Earth horizon at 63° off boresight—are 0.10% and 0.04%. The off-Earth beam fractions—beyond 63° off boresight—are 1.18% and 0.58%.

Isolation between the active and passive channels of the antenna is particularly important to the proper functioning of the radiometer. Leakage can occur in the trifrequency feed horn between its three input/output ports. These ports use standard rectangular waveguide transmission lines of type WR-62 at 13.5 GHz, type WR-42 at 22.2 GHz, and type WR-28 at 37 GHz. Leakage of the 13.5-GHz radar signal itself into either higher frequency port is negligible because it is below either of their fundamental propagating modes. Leakage of the 27-GHz second harmonic from the WR-62 port is -64.2 dB into the WR-42 port and negligible into the WR-28 port. Leakage of the 40.5-GHz third harmonic from the WR-62 port is -46.4 dB into the WR-42 port and -50.8 dB into the WR-28 port. Leakage of higher order harmonics is significantly lower than these values. The magnitude of the leakage is sufficient to potentially bias the radiometer measurements, depending on the level of harmonic suppression in the radar transmitter. For this reason, a transmit blanking capability was incorporated into the radiometer receiver design. Details of its design and performance are given in the following sections.

In order to control for and minimize thermal variations along the radiometer signal path, short sections of thin-walled stainless-steel waveguide were inserted immediately after the feed horn. These "thermal blocks" prevent the relatively large temperature excursions experienced by the feed horn from propagating toward the receivers.

B. Radiometer Receiver

A functional block diagram of one channel of the GFO WVR is shown in Fig. 2. Both the 22.2- and 37.0-GHz channels use a similar total power design. There are primary and backup (redundant) receivers for both channels to improve system reliability and increase the design lifetime. An electromechanical switch at the front of the receiver, as shown in Fig. 2, selects between primary and backup receivers. The backup receivers were fully tested and calibrated prior to launch but, to date, have not been used on orbit. The Earth-viewing input signal originates from the shared active/passive antenna. Calibration signals originate from a cold sky horn and an ambient blackbody waveguide termination. Selection between the three sources is made by latching ferrite circulators. The radiometer receivers that follow the latching circulators first mix the signals to an intermediate frequency using double-sideband downconversion, amplify them, and detect their power with square-law diodes. The receiver center frequencies and bandwidths are 22.235 GHz $\pm$ 250 MHz and 37.0 GHz $\pm$ 500 MHz, respectively. Transmit blanking is accomplished by switching the input signal source to the waveguide termination during radar pulse transmission. Guard bands in time before and after the pulse are also added, amounting to a blanking time that is approximately 12% of the total integration time.

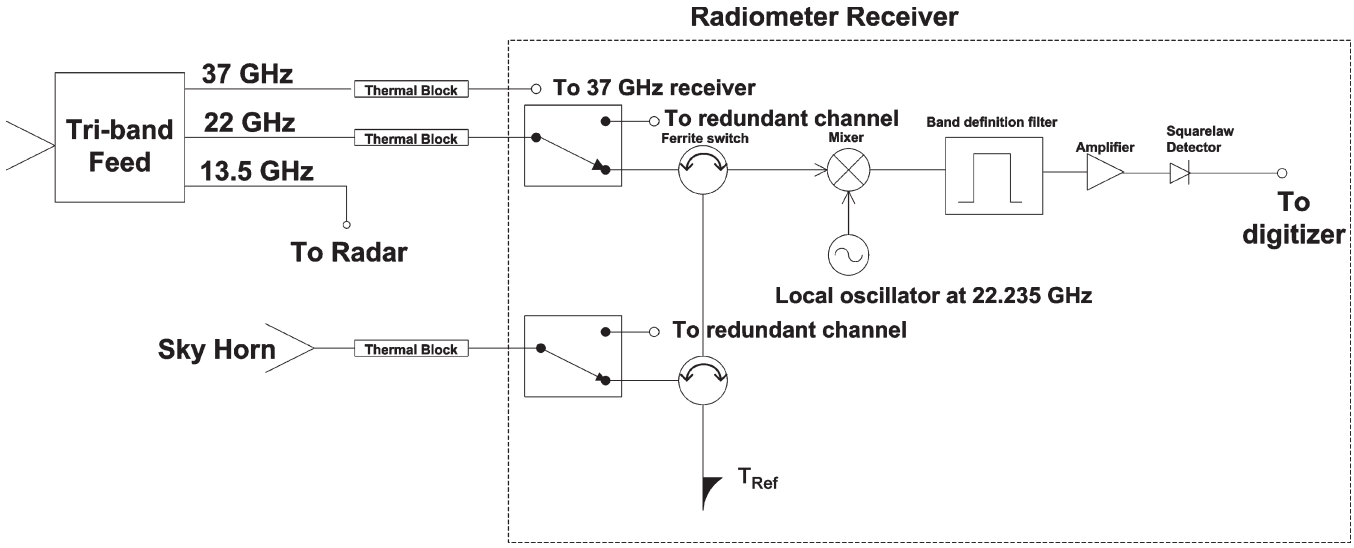

Fig. 2. GFO WVR functional block diagram. One of the 22-GHz channel receivers is shown. Redundant 22-GHz receiver and two 37-GHz receivers, which use a similar design, are not shown. Transmitter blanking is accomplished by turning both ferrite switches; thus, the receiver views the ambient reference load, which is labeled $T_{\rm ref}$ in the figure.

Integration of the detector diode signal is not disabled during transmit blanking.

A lumped-element radiative transfer forward model is used to account for losses in and thermal emission by the radiometer hardware. If T_A, T_C, and T_W are the brightness temperatures of the signals originating from the antenna, cold sky horn, and ambient (warm) calibration load, respectively, then their values after propagation through the lossy hardware are given by the primed versions

$$T'_A = \alpha_1 T_A + \alpha_2 T_f + \alpha_3 T_{\rm f.wg} + \alpha_4 T_{\rm rx} \tag{1a}$$

$$T'_C = \beta_1 T_C + \beta_2 T_h + \beta_3 T_{\rm rx} \tag{1b}$$

$$T'_W = T_W = T_{\rm rx} \tag{1c}$$

where T_f, $T_{\rm f.wg}$, $T_{\rm rx}$, and T_h are the physical temperatures of the feed horn for the main reflector, the waveguide from the feed horn to the receiver, the receiver itself, and the cold sky horn, respectively. The coefficients α_i and β_i account for losses and thermal emission, respectively, and are determined empirically by regression analysis of measurements made during thermal/vacuum testing while viewing calibration targets that provide known values for T_A and T_C.

Measurements by the radiometer are related to the expressions in (1) by

$$C_N = GT'_N + C_o \qquad N = A, C, W \tag{2}$$

where G is the receiver gain, and C_o is an offset due primarily to receiver noise temperature. The antenna temperature is calibrated from measurements of C_A, C_C, and C_W by

$$T_A = a_1 T_{\rm rx} + \frac{C_W - C_A}{C_W - C_C}(a_2 T_{\rm rx} + a_3 T_C + a_4 T_h) + a_5 T_f + a_6 T_{\rm f.wg} \tag{3}$$

where the coefficients a_i are related to the earlier coefficients by

$$a_1 = (1 - \alpha_4)/\alpha_1 \tag{4a}$$

$$a_2 = (\beta_3 - 1)/\alpha_1 \tag{4b}$$

$$a_3 = \beta_1/\alpha_1 \tag{4c}$$

$$a_4 = \beta_2/\alpha_1 \tag{4d}$$

$$a_5 = -\alpha_2/\alpha_1 \tag{4e}$$

$$a_6 = -\alpha_3/\alpha_1. \tag{4f}$$

Equations (1a)–(1c) are valid without transmit blanking. With transmit blanking enabled, (1b) and (1c) are unchanged, but (1a) becomes

$$T'_{\rm A.t} = \alpha_1(1-t)T_A + \alpha_2(1-t)T_f + \alpha_3(1-t)T_{\rm f.wg} + \alpha_4(1-t)T_{\rm rx} + tT_{\rm rx} \tag{5}$$

where t is the fractional time spent blanking the signal. If the counts measured while viewing the antenna signal during transmit blanking are denoted by $C_{\rm A.t} = GT'_{\rm A.t} + C_o$, then the corresponding calibration algorithm for the antenna temperature will be

$$T_A = a_1 T_{\rm rx} + \frac{C_W - C_{\rm A.t}}{C_W - C_C}\frac{1}{1-t}(a_2 T_{\rm rx} + a_3 T_C + a_4 T_h) + a_5 T_f + a_6 T_{\rm f.wg}. \tag{6}$$

Equations (3) and (6) are the Level 1 algorithms used to convert raw radiometer counts to calibrated antenna temperatures during on-orbit operation for the case of transmit blanking off and on, respectively.

C. Thermal/Vacuum Calibration Testing

The calibration coefficients a_i in (3) and (6), as well as the transmit blanking duty cycle t in (6), are derived by regression analysis of measurements made during thermal/vacuum testing. During the tests, temperature-controlled blackbody calibration loads were placed in front of the feed horn and cold horn. The temperature of the cold horn's calibration load was held constant at ~100 K. The temperature of the feed horn's calibration load was varied over the range ~100–325 K in steps of 30 K. The radiometer physical temperature was also varied in order to characterize temperature dependences in the calibration. The overall receiver temperature was set to 291, 298.5, and 306 K. In addition, individually controlled heater strips were attached to each of the cold horn, the feed horn, and the waveguide run from the feed horn to the receiver. These were sequentially turned on to raise the temperature of localized portions of the instrument approximately 10 K above the overall instrument.

The coefficients a_i in (3) and (6) are determined using the data taken with transmit blanking disabled. In this case, (3) is the appropriate model to calibrate the measurements. A multilinear regression was performed that solves for coefficients, which minimize the root-mean-square (rms) difference between the physical temperature of the feed horn calibration load and the temperature predicted by (3), using the data taken over the full range of the calibration load and instrument temperatures. The minimized rms differences were 0.24 and 0.19 K at 22 GHz and 0.28 and 0.21 K at 37 GHz for the primary and redundant receivers, respectively. After calibration using (3), a small quadratic nonlinearity was evident in all four receivers. It was removed by adding a small second-order correction term to (3) that depends on T_A. With this correction added, correlations between T_A and the difference between true and measured T_A are removed, and the rms differences between them are reduced to 0.07–0.09 K for the four receivers.

In order to calibrate the radiometer with transmit blanking enabled, the duty cycle t in (6) must be determined. This was done by parametrically varying its value and evaluating the resulting rms difference between true and measured values of T_A derived from the thermal/vacuum data taken with transmit blanking enabled and using (6) to calibrate the data. The results are shown in Fig. 3. A sharp minimum in the rms difference is present for each of the receivers at its optimal value for the duty cycle. The duty cycles obtained in this way are $t = 0.1140$ and 0.1142 at 22 GHz and $t = 0.1242$ and 0.1356 at 37 GHz for the primary and redundant receivers, respectively. These duty cycles are roughly consistent with the radar pulse width and prepulse and postpulse guard bands allocated to the blanking circuitry. Determination of the exact duty cycles in this empirical way ensures an accurate calibration of the antenna temperatures.

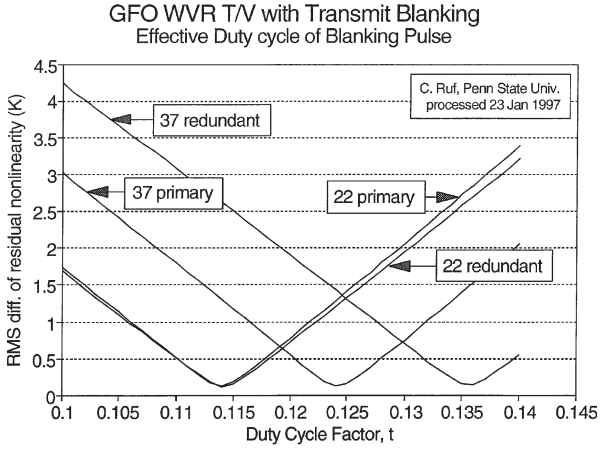

Fig. 3. RMS residual error in the GFO WVR antenna temperature calibration algorithm during prelaunch thermal/vacuum testing, with radar transmitter blanking enabled as a function of the assumed duty cycle of the blanking circuitry. The exact duty cycle is determined empirically by minimizing the error.

III. On-Orbit Evaluation

A first test of the performance of the GFO WVR on-orbit is conducted via comparisons with the TMR at crossover points in their orbits over a period of several weeks. In this and all subsequent cases except for the results presented in Section III-D, transmit blanking by the WVR is enabled, and the appropriate radiometric calibration algorithm is used. Operation with transmit blanking is the nominal mode for the WVR.

A. TOPEX Comparison

Data for use in the TMR comparison were collected from May 13 to June 21, 1998. TMR is known to be working correctly and provides path delay retrievals accurate to 1.1 cm [9]. Points where the ground track of TOPEX and GFO crossed or came within 300 km were selected for the comparison. Measurements were considered coincident provided the satellites passed over the same location within 1 h of each other. Additional constraints were used to filter the data to remove possible occurrences of ice, rain, and anomalous atmospheric and instrumental conditions. During the 40 days from which GFO data were used, there were 363 points that met all of these filtering criteria.

Fig. 4(a) shows the distribution of the distances between paired TOPEX and GFO measurements. The large number of pairs at low distances is a result of the method used to select pairs. The selection algorithm favors ground-track crossings with a relatively larger time separation over more distant approaches coincident in time. Fig. 4(b) is a similar histogram with the time difference distribution plotted. The time differences are fairly uniformly distributed over the 1-h range. Fig. 5 is a scatter plot of the pairs of GFO and TOPEX path delays. The rms difference between TOPEX and GFO is 2.7 cm, and the mean difference is 0.1 cm, with GFO biased low. A linear regression between the GFO and TOPEX data sets reveals a slope with a 95% confidence interval between 0.96 and 1.00. The fact that the confidence interval includes unity suggests that there is no statistically significant scale error between the two data sets.

The rms difference can be used to estimate GFO performance by assuming that it is composed of the following independent elements:

- TMR path delay error: 1.1 cm [9];
- Spatial decorrelation: 1.4 cm (due to an average 120-km separation [9]);

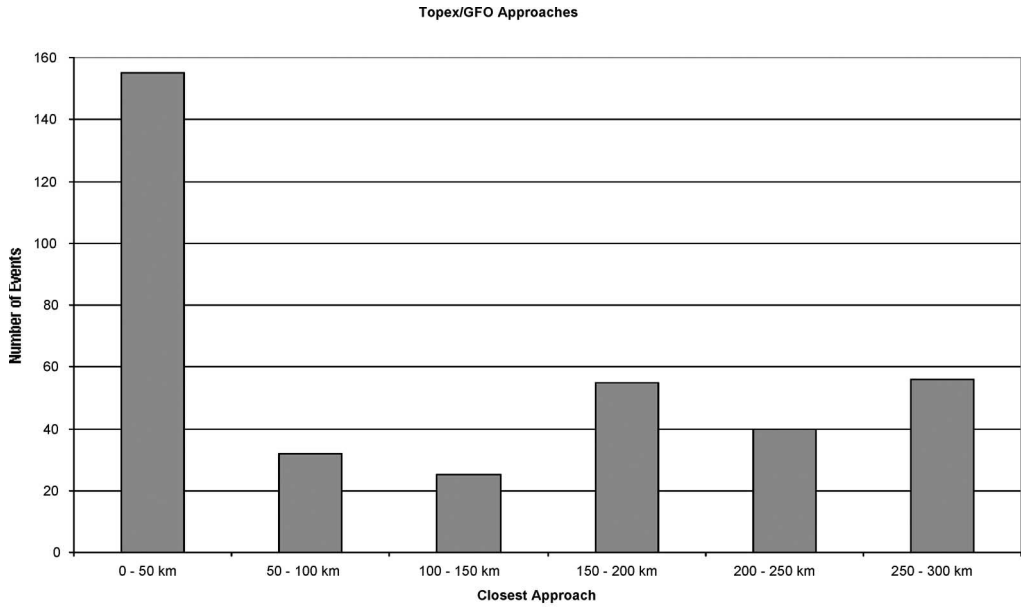

(a)

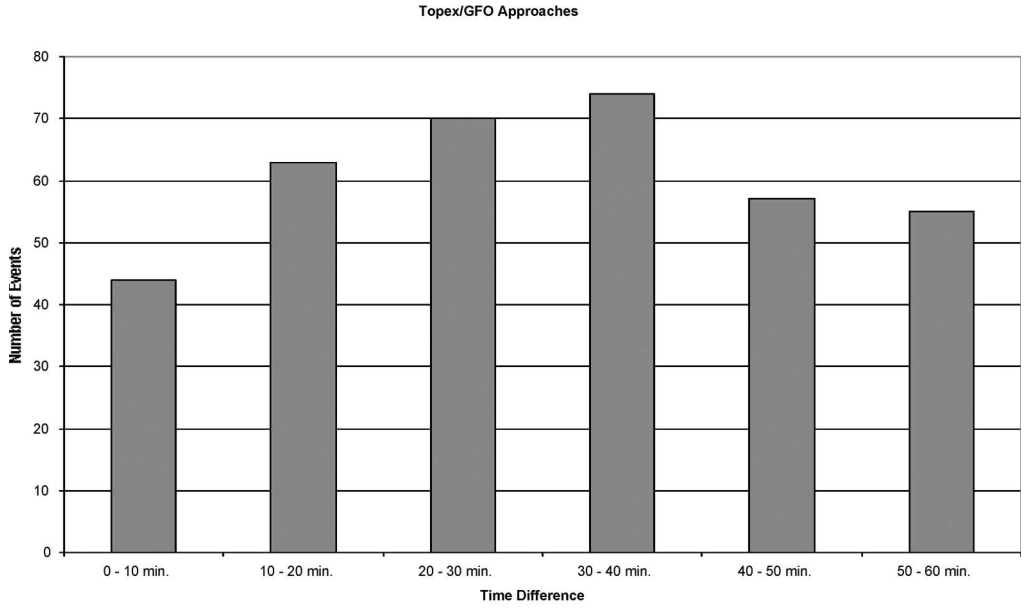

(b)

Fig. 4. Distribution of (a) separation distances and (b) time differences for the TOPEX/GFO crossovers.

- Temporal decorrelation: 0.6 cm (due to an average 30-min separation [9]);
- Wind speed correction: 0.7 cm (correction to nadir excess emissivity model [8]).

If these components are assumed to root sum square together with the GFO WVR path delay error to yield a net 2.7-cm rms difference, then the resulting WVR error is 1.8 cm.

B. Radiosonde Comparison

During the same calibration and validation (cal/val) period, a total of 263 radiosonde overpasses of 40 distinct island launch sites were recorded with separations of less than 6 h and 300 km. A map of the island launch sites is shown in Fig. 6. The wide distribution of latitudes guarantees a wide dynamic range of observed path delays. These radiosonde soundings were conducted by the national weather services of numerous countries using different humidity sensors (primarily Vaisala RS80 and RS90) and of different ages. Biases in radiosonde humidity readings have been found to depend on both sensor type and age [16], which will introduce uncertainty into the comparisons presented here.

A scatter plot of the coincident GFO WVR and radiosonde-derived path delays is shown in Fig. 7. The rms difference between the radiosonde and GFO WVR path delays in Fig. 7 is 5.4 cm. A linear regression between the two data sets reveals a slope with a 95% confidence interval between 0.94 and 0.98. This suggests the presence of a small but statistically significant scale error, which may be due to the GFO WVR and/or the aggregate of radiosonde measurements.

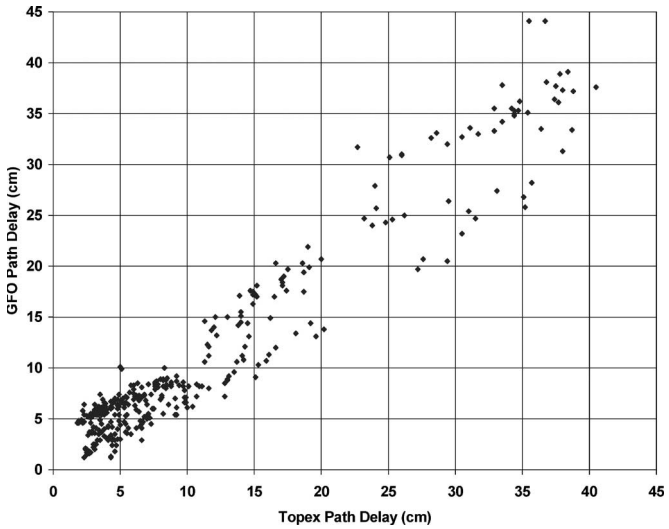

Fig. 5. Path delay comparison for the TOPEX/GFO crossovers. The rms difference between TOPEX and GFO is 2.7 cm, and the mean difference is 0.1 cm, with GFO biased low. The derived component of error due to GFO alone is 1.8 cm (see text). The slope and y intercept of the best fit linear regression are 0.98 and 0.33, respectively. The 95% confidence interval for the slope is 0.96–1.00, suggesting that there is no statistically significant scale error between TOPEX and GFO.

C. Vicarious Cold Reference Comparison

An assessment of the absolute calibration of the individual brightness temperatures at each frequency was also made by use of the vicarious cold calibration method. In summary, the manner in which the brightness temperature of the ocean varies as a function of sea surface temperature (SST), salinity (SSS), near-surface wind speed, and atmospheric opacity can be taken advantage of as a source of vicarious calibration for an orbiting microwave radiometer. For every microwave frequency, polarization, and incidence angle, there is a unique combination of SST and SSS at which the T_B of an ideal flat ocean surface is a minimum. Departures of SST and SSS from those values, as well as all variations in wind speed and atmospheric opacity, will tend to increase the T_B observed by a downward-looking radiometer in Earth orbit above its theoretical minimum. A cumulative distribution function for T_B can be constructed from a large sample of measurements, from which the highest T_B with 0% probability of occurrence can be found. This statistic is referred to as the vicarious cold T_B and has been found to be extremely stable over periods of years [11], [12]. The theoretical vicarious cold T_B are computed to be 136.4 K at 22.2 GHz (with an SST of 16.8 °C) and 152.7 K at 37.0 GHz (with an SST of 25.6 °C), using a specular ocean emission model. The values measured by GFO WVR during the cal/val effort were 136.9 and 152.6 K, respectively. These results indicate that the absolute calibration of both channels of GFO WVR was excellent during the initial cal/val period.

D. Test of Altimeter Interference and Transmitter Blanking

Prelaunch measurements of the isolation between radar and radiometer signal paths at the relevant frequencies suggest that radar interference may be small enough so that the use of transmit blanking is not necessary. Nonetheless, it was decided that the standard operating mode of the radiometer would be with transmit blanking enabled. To test this decision, the radiometer was operated briefly on orbit on March 30, 1998, without transmit blanking, from 05:40:05 to 05:41:05 universal time (UT). Shown in Fig. 8 are two time series of the 22-GHz T_B measured before, during, and after the transition to no transmit blanking. The two versions use the antenna temperature calibration algorithm with and without transmit blanking, i.e., (6) or (3). Immediately before the transition from blanking enabled to blanking disabled, the T_B is 165.0 K using (6) and 181.2 K using (3). Equation (6) is the proper calibration algorithm to use in this case. Immediately after the transition, with transmit blanking disabled, the T_B's become 146.2 and 164.6 K. In this case, the proper calibration algorithm has changed to (3). The properly calibrated T_B has thus changed by only 0.4 K. Similarly for the transition 1 min later back to transmit blanking enabled, the properly calibrated T_B is 179.0 K just before the transition and 178.6 K just after. The change is again 0.4 K, but not in the reverse direction. This suggests that the change is not due to a persistent bias between the two algorithms. It is more likely a result of additive noise effects and/or geophysical variations in T_B from 1 s to the next. In any event, the changes are quite small and suggest that any leakage there may be of the radar signal into the radiometer is likewise small.

E. Long-Term Mission Performance Assessment

The operational phase of the GFO mission began in November 2000. Beginning at that time and continuing on to the present, performance of the GFO WVR has been assessed each orbit repeat cycle (every 17 days) by evaluating the vicarious cold T_B at 22.2 and 37.0 GHz. A time series of the vicarious cold T_B at each frequency is shown in Fig. 9 for the period from November 30, 2000, to May 26, 2006. The average values over the full period are 135.7 K (22.2 GHz) and 152.1 K (37.0 GHz). These values are nearly identical to those determined during the earlier cal/val phase. The standard deviations of the vicarious cold T_B over the full time interval are 0.63 and 0.35 K, respectively. This indicates that the instrument has had a stable absolute calibration at the $\sim$0.4 K level or better for the life of the mission. It is likely that the higher variability noted at 22.2 GHz is due not to the instrument but to the inherent sensitivity of the vicarious cold method to seasonal water vapor variations in the atmosphere.

The performance and health of the GFO WVR can also be monitored via the white noise standard deviation (WNSD) present on 1-s integration retrievals of the path delay and measurements of the individual brightness temperatures. Estimates of the WNSD are made directly from the Earth-viewing measurements and, thus, are a good indicator of the system noise temperature of the radiometer electronics while viewing the Earth. The WNSD of the 22.2- and 37.0-GHz brightness temperatures has also been estimated cycle-by-cycle from November 30, 2000, to May 26, 2006. The WNSD for both channels has been steady for the life of the mission. The average of WNSD over all cycles for the complete mission lifetime life is 0.20 K (22 GHz) and 0.14 K (37.0 GHz). These values are consistent with the prelaunch results, indicating that

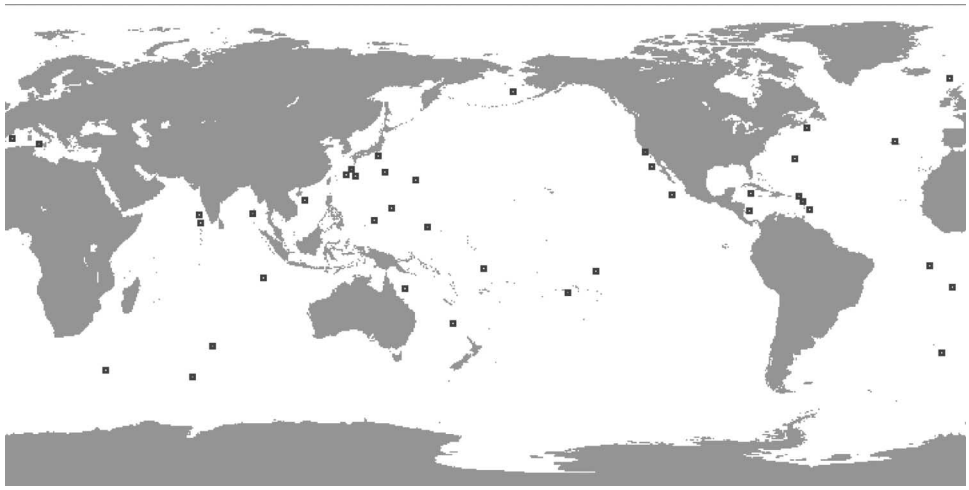

Fig. 6. Locations of the 40 active island radiosonde launch sites that were operating during the GFO WVR cal/val period from May 13 to June 21, 1998. The wide distribution of latitudes guarantees an acceptable dynamic range of observed path delays.

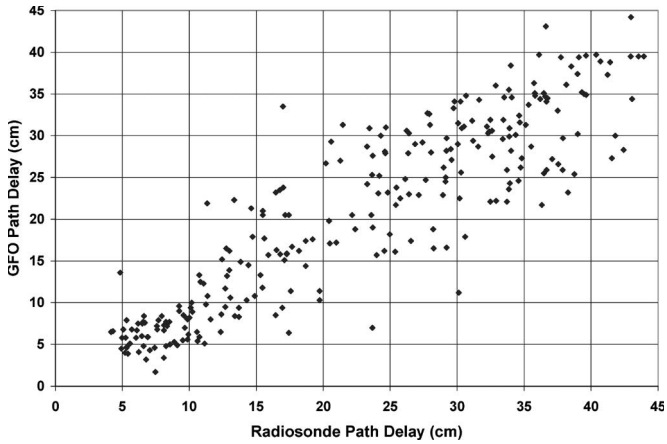

Fig. 7. Scatter plot of coincident path delays measured by the island-launched radiosondes and retrieved by the GFO WVR from May 13 to June 21, 1998. The rms difference between the two data sets is 5.4 cm. The slope and y intercept of the best fit linear regression are 0.96 and -0.98, respectively. The 95% confidence interval for the slope is 0.94–0.98, suggesting that there may be a statistically significant scale error due to errors in the GFO WVR and/or radiosondes.

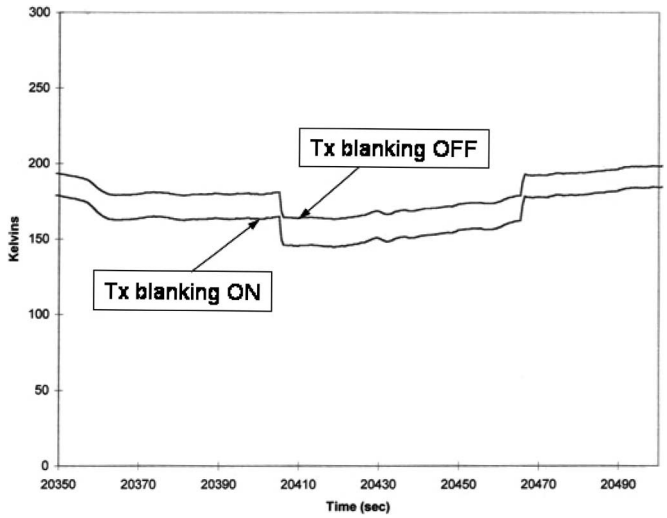

Fig. 8. Time series of GFO WVR 22.2-GHz brightness temperature measurements using calibration algorithms that assume transmit blanking is or is not enabled. The nominal operating mode is *with* transmit blanking, so that the algorithm without blanking yields erroneously high values. For approximately 1 min of on-orbit operation, on March 30, 1998, from 05:40:05 to 05:41:05 UT, transmit blanking was disabled. The fact that the brightness temperature tracks so closely across the transitions between transmit blanking states indicates that isolation between the radar and radiometer is sufficiently high that the blanking was probably not necessary.

the system noise temperature and noise figure of the receiver electronics have themselves remained steady at their prelaunch values throughout the mission lifetime. The WNSD of the path delay estimates that are derived from the 22.2- and 37.0-GHz brightness temperatures has remained below the 0.15-cm level for the entire mission. This is the threshold performance limit below which GFO WVR is intended to operate.

IV. Conclusion and Discussion

The shared-antenna design used by the GFO radar altimeter and WVR has been shown to have no significant detrimental effect on radiometer performance. WVR performance was assessed on orbit using intercomparisons with colocated radiosonde soundings, with matchups with another well-calibrated spaceborne radiometer, and with statistical analysis of a vicarious cold brightness temperature reference. The long-term stability of WVR calibration was also evaluated using the vicarious cold reference method, and it was found to be drift free at the several tenths of kelvin levels over the full 8+ years of the GFO mission life to date.

The WVR uses a transmit blanking approach that switches the radiometer input signal away from the antenna (and any potential radar interference) during and shortly before and after the transmission of each radar pulse. This reduces the effective duty cycle of Earth observations by the radiometer by 11%–14% and therefore raises the noise-equivalent (NE) ΔT of the observations by approximately 6%. A modification to the antenna temperature calibration algorithm is presented, which accounts for the transmit blanking. It is shown to produce calibrated antenna temperatures that are comparable to the case without transmit blanking. A brief test while on orbit of the need for transmit blanking was conducted. The results suggest

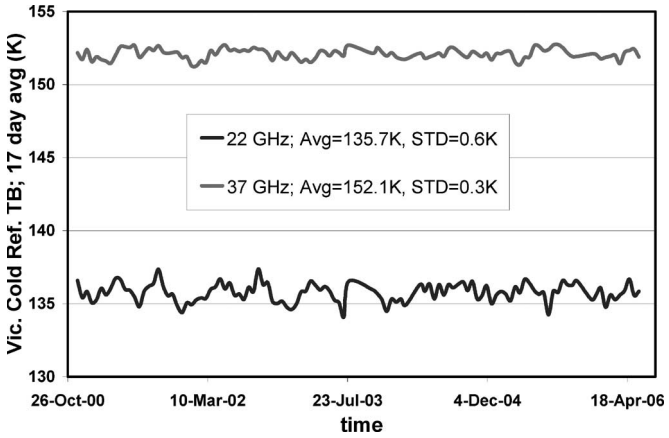

Fig. 9. Time series of the vicarious cold reference brightness temperature measured by the GFO WVR at 22.2 and 37.0 GHz from November 30, 2000, to May 26, 2006. The fact that this reference is flat indicates that there is no systematic drift in radiometer calibration over the life of the mission.

that isolation between the radar and radiometer was likely sufficient to obviate the need for blanking. Nonetheless, the standard operational mode of the radiometer is with transmit blanking enabled. The increase in NE ΔT with blanking did not substantively affect the quality of the WVR wet path delay retrievals, and the blanking added an extra layer of protection of the radiometer from the radar.

ACKNOWLEDGMENT

The authors would like to thank members of the GFO team for their support and assistance, in particular G. Alikakos (EDO) with the WVR receivers, L. Diaz (BATC) with the antenna design, J. Finkelstein (GFO Project) with postlaunch cal/val, C. Kilgus (GFO Project) with prelaunch and postlaunch support, and M. Rau (GFO Project) with postlaunch cal/val. The frequency channel selection used by the GFO WVR was initially proposed by a team at the Naval Research Laboratory led by V. E. Noble.

REFERENCES

[1] R. Barry, J. Finkelstein, C. Kilgus, C. N. K. Mooers, B. Needham, and M. Crawford, "GEOSAT Follow-On satellite to supply ocean sciences data," *EOS Trans. AGU*, vol. 76, no. 4, pp. 23–26, Jan. 24, 1995.

[2] R. Bernard, A. Le Cornec, L. Eymard, and L. Tabary, "The microwave radiometer aboard ERS-1: Part 1—Characteristics and performance," *IEEE Trans. Geosci. Remote Sens.*, vol. 31, no. 6, pp. 1186–1198, Nov. 1993.

[3] S. Brown, C. Ruf, S. Keihm, and A. Kitiyakara, "Jason microwave radiometer performance and on-orbit calibration," *Mar. Geod.*, vol. 27, no. 1/2, pp. 199–220, 2004.

[4] R. E. Cheney, B. C. Douglas, R. W. Agreen, L. Miller, D. L. Porter, and N. S. Doyle, "GEOSAT altimeter geophysical data user handbook," Nat. Ocean. Serv., Rockville, MD, NOAA Tech. Memo, NOS NGS-46, 1987.

[5] J. C. Giampaolo, "An improved ocean surface emissivity wind speed correction," M.S. thesis, Penn State Univ., University Park, PA, 1999.

[6] S. J. Keihm, M. A. Janssen, and C. S. Ruf, "TOPEX/Poseidon microwave radiometer (TMR): III. Wet troposphere range correction algorithm and pre-launch error budget," *IEEE Trans. Geosci. Remote Sens.*, vol. 33, no. 1, pp. 147–161, Jan. 1995.

[7] D. Prabhakara, H. D. Chang, and A. T. C. Chang, "Remote sensing of precipitable water over the oceans from Nimbus 7 microwave measurements," *J. Appl. Meteorol.*, vol. 21, no. 1, pp. 59–68, Jan. 1982.

[8] C. S. Ruf, R. P. Dewan, and B. Subramanya, "Combined microwave radiometer and altimeter retrieval of wet path delay for the GEOSAT Follow On," *IEEE Trans. Geosci. Remote Sens.*, vol. 34, no. 4, pp. 991–999, Jul. 1996.

[9] C. S. Ruf, S. J. Keihm, B. Subramanya, and M. A. Janssen, "TOPEX/Poseidon microwave radiometer performance and in-flight calibration," *J. Geophys. Res.*, vol. 99, no. C12, pp. 24 915–24 926, Dec. 1994.

[10] C. S. Ruf, M. A. Janssen, and S. J. Keihm, "TOPEX/POSEIDON Microwave Radiometer (TMR): I. Instrument description and antenna temperature calibration," *IEEE Trans. Geosci. Remote Sens.*, vol. 33, no. 1, pp. 125–137, Jan. 1995.

[11] C. S. Ruf, "Detection of calibration drifts in spaceborne microwave radiometers using a vicarious cold reference," *IEEE Trans. Geosci. Remote Sens.*, vol. 38, no. 1, pp. 44–52, Jan. 2000.

[12] ——, "Characterization and correction of a drift in calibration of the TOPEX Microwave Radiometer," *IEEE Trans. Geosci. Remote Sens.*, vol. 40, no. 2, pp. 509–511, Feb. 2002.

[13] J. Stum, "A comparison of the brightness temperatures and water vapor path delays measured by the TOPEX, ERS-1, and ERS-2 microwave radiometers," *J. Atmos. Ocean. Technol.*, vol. 15, no. 4, pp. 987–994, Aug. 1998.

[14] B. D. Tapley, J. B. Lundberg, and G. H. Born, "The SeaSat altimeter wet tropospheric range correction," *J. Geophys. Res.*, vol. 87, no. C5, pp. 3213–3220, Apr. 1982.

[15] F. J. Wentz, "A model function for ocean microwave brightness temperatures," *J. Geophys. Res.*, vol. 88, no. C3, pp. 1892–1908, 1983.

[16] E. R. Westwater, B. B. Stankov, D. Cimini, Y. Han, J. A. Shaw, B. M. Lesht, and C. N. Long, "Radiosonde humidity soundings and microwave radiometers during Nauru99," *J. Atmos. Ocean. Technol.*, vol. 20, no. 7, pp. 953–971, Jul. 2003.

Christopher S. Ruf (S'85–M'87–SM'92–F'01) received the B.A. degree in physics from Reed College, Portland, OR, and the Ph.D. degree in electrical and computer engineering from the University of Massachusetts, Amherst.

He is currently a Professor of Atmospheric, Oceanic, and Space Sciences and Electrical Engineering and Computer Science, and the Director of the Space Physics Research Laboratory, Department of Atmospheric, Oceanic, and Space Sciences, University of Michigan, Ann Arbor. He has been with Intel Corporation, Hughes Space and Communications, the National Aeronautics and Space Administration Jet Propulsion Laboratory, and the Pennsylvania State University, University Park. During 2000, he was a Guest Professor at the Technical University of Denmark, Lyngby, Denmark. He has published more than 98 refereed articles, primarily in the area of microwave remote sensing. He has served on the editorial boards of *Radio Science* and the *Journal of Atmospheric and Oceanic Technology*.

Dr. Ruf has received three NASA Certificates of Recognition [1990 and 1992 (2)] and four NASA Group Achievement Awards [1993 (2), 1994, and 2004], as well as the 1997 GRS-S Transactions Prize Paper Award and the 1999 IEEE Judith A. Resnik Technical Field Award. He serves on the editorial boards of the IEEE GEOSCIENCE AND REMOTE SENSING (GRS-S) NEWSLETTER and the IEEE TRANSACTIONS ON GEOSCIENCE AND REMOTE SENSING. He is a member of the American Geophysical Union, the American Meteorological Society, and Commission F of the International Scientific Radio Union.

April M. Warnock is currently working toward the B.S. degree in atmospheric, oceanic, and space sciences, with a meteorology concentration, at the University of Michigan, Ann Arbor.

She is a member of the Microwave Remote Sensing Group, Space Physics Research Laboratory, Department of Atmospheric, Oceanic, and Space Sciences, University of Michigan.